Available online at www.sciencedirect.com
ScienceDirect
C. R. Physique 10 (2009) 54–64
COMPTES RENDUS PHYSIQUE

New approaches in Electromagnetic Compatibility / Nouvelles approches en Compatibilité Electromagnétique

Numerical simulation of a Reverberation Chamber with a stochastic collocation method

Pierre Bonnet [a,*], Fatou Diouf [a], Cédric Chauvière [b], Sébastien Lalléchère [a], Michel Fogli [c], Françoise Paladian [a]

[a] *LASMEA, UMR 6602, Université Blaise-Pascal, Les Cézeaux, 63177 Aubière cedex, France*
[b] *LM, UMR 6620, Université Blaise-Pascal, Les Cézeaux, 63177 Aubière cedex, France*
[c] *LaMI, EA 3867, Université Blaise-Pascal, Les Cézeaux, 63177 Aubière cedex, France*

Available online 17 March 2009

Abstract

An original numerical modelling of Mode Stirred Reverberation Chamber used in Electromagnetic Compatibility is proposed. This method relies on an analogy between a reverberation chamber and an enclosure whose walls' conductivity is randomly characterised. The distribution law of this parameter is obtained by measurements. Applying a stochastic collocation method enables one to numerically assess electromagnetic field from a low number of empty cavity (without stirrer) simulations. Thus this approach notably reduces CPU time allowing more complex simulations. ***To cite this article: P. Bonnet et al., C. R. Physique 10 (2009).***

Résumé

Simulation numérique d'une chambre réverbérante par une méthode de collocation stochastique. Cet article propose une méthodologie originale pour la modélisation numérique de Chambres Réverbérantes à Brassage de Modes utilisées en Compatibilité Electromagnétique. Cette approche repose sur une analogie entre une chambre réverbérante et une cavité dont les parois sont caractérisées par une conductivité aléatoire. La loi de distribution de ce paramètre est établie à partir de mesures. L'application d'une méthode de collocation stochastique permet alors de déterminer numériquement le champ électromagnétique grâce à un faible nombre de simulation d'une cavité sans brasseur. Cette méthodologie conduit ainsi à une amélioration importante en temps de calcul autorisant des simulations plus complexes. ***Pour citer cet article : P. Bonnet et al., C. R. Physique 10 (2009).***

Keywords: EMC; Reverberation Chamber; Stochastic collocation; Stochastic field

Mots-clés : CEM ; Chambre réverbérante ; Collocation stochastique ; Champ stochastique

* Corresponding author.
E-mail addresses: bonnet@lasmea.univ-bpclermont.fr (P. Bonnet), diouf@lasmea.univ-bpclermont.fr (F. Diouf), chauviere@math.univ-bpclermont.fr (C. Chauvière), lallechere@lasmea.univ-bpclermont.fr (S. Lalléchère), m.fogli@cust.univ-bpclermont.fr (M. Fogli), paladian@lasmea.univ-bpclermont.fr (F. Paladian).

1631-0705/$ – see front matter
doi:10.1016/j.crhy.2008.12.001

1. Introduction

Reverberation Chambers (RC or MSRC for mode-stirred reverberation chambers) are efficient tools for Electromagnetic Compatibility (EMC) tests [1,2]. They usually provide a simple way to obtain good field uniformity using an easy-to-build structure at reasonable cost. A reverberation chamber is generally a shielded enclosure with metallic walls and one or several stirrers. The stirrer, usually in the form of a paddle wheel, varies the chamber's boundary conditions to provide a statistically uniform environment. For optimisation or better understanding of the behaviour of a RC, numerical modelling by frequential [3,4] or temporal methods [5–8] is meeting growing interest. If one observes suitable comparisons between theory and experimentation, these results nevertheless are obtained at high computing costs. Indeed, reproducing experimental conditions requires to take into account the revolution of the stirrer. To obtain an ideal stirring, stirrers need to be complex. Unfortunately, for most volumic temporal approaches like those based upon classical Finite Difference or TLM methods, Cartesian spatial griding reveals as a major difficulty. This problem may be handled by 3-D frequency techniques (discretisation in surfaces). Nevertheless, previous models are more expensive in terms of CPU time and an accurate description of the stirrer will lead to impossible insertion of equipment under test. Thus it may seem interesting to withdraw modelling of the stirrer without altering representativeness of electromagnetic fields inside the studied MSRC. In this way, accurate probabilistic methods may represent an alternative to deterministic techniques. In this article, a probabilistic model is developed: the aim is to assimilate a MSRC with a stirrer to an empty cavity for which the walls conductivity is randomly taken. The probability law of this random variable will be established from measured results and a formalism is validated at high frequencies. This conductivity model will then be integrated to solve Maxwell equations with a stochastic collocation method. The use of such technique enables MSRC simulations with no stirrer, and furthermore real losses observed in MSRC may be integrated directly in FDTD. This complete process shows that a low number of simulations without any stirrer may reveals as efficient as a full deterministic description of MSRC in order to settle first order moments of electric field generated in the working volume.

2. Probabilistic model for MSRC

MSRC enables one to generate an electromagnetic environment characterised by a field distribution considered as statistically homogeneous and isotropic with random polarisation. In order to achieve EMC tests, it is necessary to do measurements for N independent configurations. These environments correspond to the different boundary conditions occurring inside the structure, for a given excitation frequency. When this number N, corresponding to stirrer steps, tends to infinity, the properties of the internal electromagnetic field in the CRBM are identical whatever the point considered inside the structure: every direction and every polarisation are equiprobable.

The unpredictable character of the polarisation and the statistical isotropy of the field are obtained in a MSCR by producing unpredictable modifications of spatial distributions of the field. One of the most important parameters charactering MSRC is its quality factor. At high frequencies, this parameter corresponds to the partial quality factor concerning the losses by the Joule effect in the walls of the cavity. Moreover, at frequencies for which the internal electromagnetic field is statistically uniform, we have [9]

$$Q = \frac{3V}{2S\delta} = \frac{\omega\epsilon_0 |E_0|^2 V}{P_{\text{trans}}} \tag{1}$$

where V and S stand for the volume and the area of all the metallic surfaces of the MSRC, δ is the skin depth, P_{trans} represents the power transmitted to MSRC. Conductivity of walls is also linked, for a given frequency, to the magnitude of total electric field $|E_0|$ generated inside working volume of MSRC by

$$\sigma = \frac{S^2 f}{2916\pi^2 10^{11} |E_0|^4 / P_{\text{trans}}^2} \tag{2}$$

The conductivity is a deterministic physical parameter. For a fixed stirrer position, reverberation is a deterministic process, its evolution in time (EMC test) is both repeatable and reproducible when initial conditions are kept from one test to the other. In other words, when steps of stirrer and positions of equipment under test are set, measured results must be equal (with slight differences due to uncertainties of measurement). In fact, the pseudo random characteristics of data appear "inside" a test, considering each step of the stirrer like an electromagnetic environment; the whole space

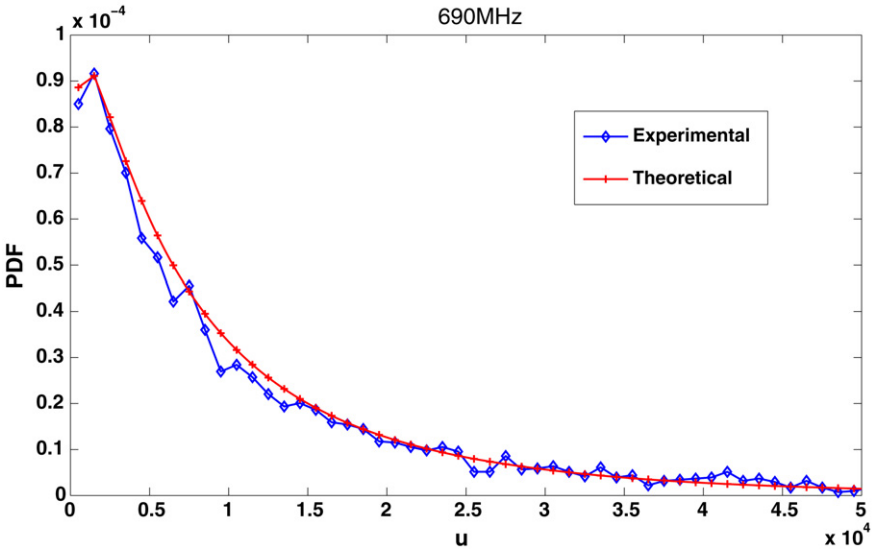

Fig. 1. PDF of the conductivity at 690 MHz in LASMEA MSRC.

distributions of the electromagnetic field are generated over a complete rotation of the stirrer. Ideally, for an infinite number of steps of the stirrer, one experiment includes one process justifying the use of statistic methods. Nevertheless, practically, the number of steps is finite; thus, experimental conditions do not fit with ideal characteristics. This is the reason why theoretical methods must be developed in order to model in an efficient and realistic way a deterministic EMC test. For a given frequency and for each step of the stirrer, boundary conditions of MSRC are modified; thus the main assumption relies on "virtual" variation of the conductivity from one position of the stirrer to the other. This last hypothesis suggests that all uncertainties (any uncontrolled physical phenomena in MSRC) are contained in this parameter.

It is to be noticed that the probabilistic model proposed in this article does not aim to reproduce field's behaviour for each step of the stirrer, but to evaluate second order moments of electromagnetic quantities by a "simple" technique (no requirement of "heavy" simulations of MSRC, for instance without stirrer).

From Eq. (2) and Hill's results concerning $|E_0|$ [9], it can be established that the conductivity σ which varies with frequency, follows a χ^4_6 distribution and its probability density function (pdf), its mean and its standard deviation being given by

$$P_\sigma(u) = \frac{\sqrt{u}\, e^{-\frac{1}{2}\sqrt{u/(b_f s^4)}}}{32(b_f s^4)^{\frac{3}{2}}} 1_{\mathbb{R}_+^*}(u) \tag{3}$$

$$m_\sigma = 48 b_f s^4 \tag{4}$$

$$s_\sigma = 24\sqrt{6} b_f s^4 \tag{5}$$

with

$$b_f = \frac{S^2 f}{8100\pi\mu_0 c^2 P_t^2}$$

and s is the standard deviation of the complex electric field components. In order to assess these results, many measurements of the electric field were obtained in the LASMEA MSRC working volume (sizes: 8.40 m × 6.70 m × 3.50 m). In the frequency range from 250 MHz to 1 GHz with a 10 MHz frequency step, $|E_0|$ was measured for 80 points and 51 positions of the stirrer. Consequently, from (2), 4080 values of conductivities are available for each frequency of the study. Theoretical and experimental pdf match well as shown on Fig. 1 at 690 MHz (similar results are obtained from 400 MHz and up to 1 GHz).

3. Choice of the output

3.1. Coefficient of variation

From previous measurements, the aim is to numerically reproduce the experimental setup and to assess the mean value of the electric field magnitude over a full revolution of the stirrer for a given number of points located inside the working volume of the chamber. The output of interest is the coefficient of variation (CV) defined by the ratio of standard deviation and mean of the total electric field magnitude. The advantage given by this parameter is that it remains independent from the power transmitted to MSRC.

Moreover, contrary to experiments where only magnitude of field components may be obtained (with the help of a triaxial sensor), it is possible to get real and imaginary parts of field numerically. In order to have at one's disposal a theoretical value for the coefficient of variation, the case of an empty chamber is considered.

It can be shown that the modulus $|\hat{\mathbf{E}}_p|$ of every component $\hat{\mathbf{E}}_p$ of the total electric field $\hat{\mathbf{E}}$ follows a Rayleigh distribution of order 2 with scaling factor whose coefficient of variation is given by

$$CV_{|\hat{\mathbf{E}}_p|} = \frac{s_{e|\hat{\mathbf{E}}_p|}\sqrt{2-\pi/2}}{s_{m|\hat{\mathbf{E}}_p|}\sqrt{\pi/2}} \approx 0.5227 \tag{6}$$

where $s_{e|\hat{\mathbf{E}}_p|}$ and $s_{m|\hat{\mathbf{E}}_p|}$ are two coefficients > 0 ideally equal [10].

It can also be shown that the magnitude $\|\hat{\mathbf{E}}\|$ of the total electric field $\hat{\mathbf{E}}$ follows a Rayleigh distribution of order 6 with scaling factor whose coefficient of variation is given by

$$CV_{\|\hat{\mathbf{E}}\|} = \frac{s_{e\|\hat{\mathbf{E}}\|}\sqrt{6-225\pi/128}}{s_{m\|\hat{\mathbf{E}}\|}15\sqrt{2\pi}/16} \approx 0.294 \tag{7}$$

where $s_{e\|\hat{\mathbf{E}}\|}$ and $s_{m\|\hat{\mathbf{E}}\|}$ are also two strictly positive coefficients ideally equal [10].

Obviously, the coefficient of variation of the electric field in a real MSRC is different from that generated inside an ideal chamber (presence of various losses due to the frame and uncertainties in measurements). These losses and uncertainties will have an impact on the scaling factor of the coefficient of variation.

3.2. Application to LASMEA MSRC

From previous measurements, the coefficient of variation of LASMEA MSRC was obtained from 80 sensors equally distributed inside the working volume. Since each value of the electric field magnitude may be related to one value of the conductivity from (2), the inner electric field may be established numerically to simulate a lossy cavity without stirrer. From the large number of numerical methods available to handle the problem, a combination of FDTD technique and a Surface impedance Boundary Condition (SIBC) [11] modelling (insertion of conductivities) has been chosen. Results given on Fig. 2 show a comparison between coefficient of variation at 620 MHz obtained respectively from: (i) measurements; (ii) numerical results simulated for 51 conductivities (linked to 51 positions of the stirrer) coming from measured $|E_0|$ at one point and (2); and (iii) simulations achieved for 4080 available values of conductivity.

Results given by 51 and 4080 simulations (those requiring important CPU time) are close to the approached theoretical value. However, this methodology does not take into account the law of probability of conductivity, which is the reason why the study is orientated towards a probabilistic approach for more realistic and efficient simulations.

4. Simulation of MSRC by a stochastic collocation method

The use of Monte Carlo type methods for the simulation of a cavity with walls having a random conductivity is also possible. However, this method being easy to implement, and making use of possible deterministic codes, exhibits very slow rates of convergence ($\sim N^{-1/2}$, if N is the number of simulated realisations). This is why, over the last few years, other numerical methods have appeared, among which, the stochastic collocation method [12].

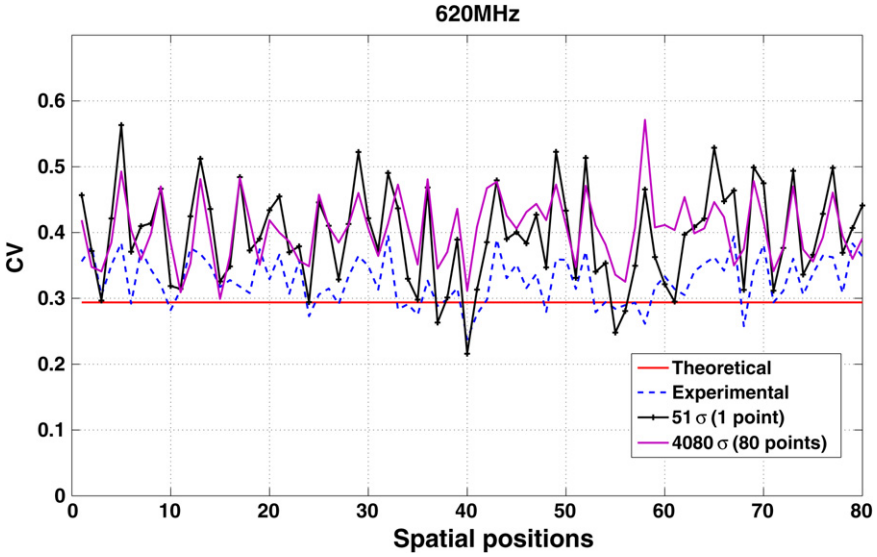

Fig. 2. Coefficient of variation for 80 points into the working volume.

When applied to Maxwell's equations, this enables a direct computation of the statistics of the electric field and the magnetic field in the cavity. Moreover, a limited number of collocation points – and thus simulations – is sufficient to get the convergence of results.

4.1. Resolution of Maxwell's equations by a stochastic collocation method

For every point (x, y, z) of an homogeneous and isotropic domain, and at any time t, Maxwell's linear equations can be written:

$$\begin{cases} \epsilon \dfrac{\partial \mathbf{E}}{\partial t} - \nabla \times \mathbf{H} + \sigma \mathbf{E} = 0 \\ \mu \dfrac{\partial \mathbf{H}}{\partial t} + \nabla \times \mathbf{E} = 0 \end{cases} \tag{8}$$

where σ is the previously defined random variable, which follows a χ^4_6 probability distribution with parameters given by Eq. (3).

The electric fields and the magnetic fields are functions of this random variable and they are denoted, respectively, by $\mathbf{E}(t; x, y, z; \sigma)$ and $\mathbf{H}(t; x, y, z; \sigma)$. Here, the values of interest are the second order statistics of the electric field $\mathbf{E}(t; x, y, z; \sigma)$, and more specifically of its spectral dual $\hat{\mathbf{E}}(f; x, y, z; \sigma)$. The idea is to approximate the stochastic fields $\mathbf{E}(t; x, y, z; \sigma)$ and $\mathbf{H}(t; x, y, z; \sigma)$ by projecting them onto a Lagrange basis, i.e.

$$\begin{cases} \mathbf{E}(t; x, y, z; \sigma) \simeq \displaystyle\sum_{i=0}^{n} \mathbf{E}^i(t; x, y, z) L_i(\sigma) \\ \mathbf{H}(t; x, y, z; \sigma) \simeq \displaystyle\sum_{i=0}^{n} \mathbf{H}^i(t; x, y, z) L_i(\sigma) \end{cases} \tag{9}$$

where $n \geqslant 0$ is a given integer number and, L_i $(0 \leqslant i \leqslant n)$, are Lagrange polynomials of degree n defined by

$$L_i(u) = \prod_{j=0}^{n} \frac{u - \sigma_j}{\sigma_i - \sigma_j} \tag{10}$$

where σ_j, $0 \leqslant j \leqslant n$, are the collocation points associated with the probability density function (pdf) of σ.

These polynomials possess the important property

$$\forall (i, j) \in \{0, \ldots, n\}^2, \quad L_i(\sigma_j) = \delta_{ij} \tag{11}$$

where δ_{ij} is the Kronecker delta.

The $n+1$ points σ_j $(0 \leqslant j \leqslant n)$, are obtained from the pdf of σ [12]. For reason of simplicity, the n-approximations $(\mathbf{E}_n, \mathbf{H}_n)$ of the fields $(\mathbf{E}, \mathbf{H})$, such that

$$\begin{cases} \mathbf{E}_n(t; x, y, z; \sigma) = \displaystyle\sum_{i=0}^{n} \mathbf{E}^i(t; x, y, z) L_i(\sigma) \\ \mathbf{H}_n(t; x, y, z; \sigma) = \displaystyle\sum_{i=0}^{n} \mathbf{H}^i(t; x, y, z) L_i(\sigma) \end{cases} \tag{12}$$

are denoted by $(\mathbf{E}, \mathbf{H})$ again in the following. The unknowns of the problem are the $n+1$ couples $(\mathbf{E}^i(t; x, y, z), \mathbf{H}^i(t; x, y, z))$ $(0 \leqslant i \leqslant n)$, denoted by $(\mathbf{E}^i, \mathbf{H}^i)$.

Setting $\mathbf{E}_n = \mathbf{E}$ and $\mathbf{H}_n = \mathbf{H}$ into the relation (12) and inserting these relations into Eq. (8), we obtain

$$\begin{cases} \displaystyle\sum_{i=0}^{n} \left(\epsilon \frac{\partial \mathbf{E}^i}{\partial t} - \nabla \times \mathbf{H}^i + \sigma \mathbf{E}^i \right) L_i(\sigma) = 0 \\ \displaystyle\sum_{i=0}^{n} \left(\mu \frac{\partial \mathbf{H}^i}{\partial t} + \nabla \times \mathbf{E}^i \right) L_i(\sigma) = 0 \end{cases} \tag{13}$$

Taking $\sigma = \sigma_j$ in the above equations and using (11), we get (for $0 \leqslant j \leqslant n$)

$$\begin{cases} \displaystyle\sum_{i=0}^{n} \left(\epsilon \frac{\partial \mathbf{E}^i}{\partial t} - \nabla \times \mathbf{H}^i + \sigma_j \mathbf{E}^i \right) \delta_{ij} = 0 \\ \displaystyle\sum_{i=0}^{n} \left(\mu \frac{\partial \mathbf{H}^i}{\partial t} + \nabla \times \mathbf{E}^i \right) \delta_{ij} = 0 \end{cases} \tag{14}$$

and therefore

$$\begin{cases} \epsilon \dfrac{\partial \mathbf{E}^i}{\partial t} - \nabla \times \mathbf{H}^i + \sigma_i \mathbf{E}^i = 0 \\ \mu \dfrac{\partial \mathbf{H}^i}{\partial t} + \nabla \times \mathbf{E}^i = 0 \end{cases} \tag{15}$$

with $0 \leqslant i \leqslant n$.

We are now led to solve $n+1$ deterministic problems, for which efficient numerical methods exist. The same previous SIBC-type methods used for deterministic FDTD simulations was employed.

Once these equations have been solved, the $n+1$ functions $(\mathbf{E}^i(t; x, y, z), \mathbf{H}^i(t; x, y, z))$, $0 \leqslant i \leqslant n$, are known and the approximate stochastic solution $(\mathbf{E}_n, \mathbf{H}_n)$ given by Eq. (12) is entirely specified. Then, after a Fourier transform, we obtain its dual spectral $(\hat{\mathbf{E}}_n, \hat{\mathbf{H}}_n)$ such that

$$\begin{cases} \hat{\mathbf{E}}_n(f; x, y, z; \sigma) = \displaystyle\sum_{i=0}^{n} \hat{\mathbf{E}}^i(f; x, y, z) L_i(\sigma) \\ \hat{\mathbf{H}}_n(f; x, y, z; \sigma) = \displaystyle\sum_{i=0}^{n} \hat{\mathbf{H}}^i(f; x, y, z) L_i(\sigma) \end{cases} \tag{16}$$

where $\hat{\mathbf{E}}^i$ and $\hat{\mathbf{H}}^i$ denote the Fourier transforms of $\mathbf{E}^i$ and $\mathbf{H}^i$, respectively. The couple $(\hat{\mathbf{E}}_n, \hat{\mathbf{H}}_n)$ is an n-approximation of the dual spectral $(\hat{\mathbf{E}}, \hat{\mathbf{H}})$ of the exact solution $(\mathbf{E}, \mathbf{H})$ of Eq. (8). It is denoted by $(\hat{\mathbf{E}}, \hat{\mathbf{H}})$ in the following.

4.2. Computation of statistics of the stochastic field

4.2.1. Computation of the mean

By definition, the mean of the random field $\hat{\mathbf{E}}$ is given by

$$m_{\hat{\mathbf{E}}}(f;\mathbf{r}) = \int_{\mathbb{R}} \hat{\mathbf{E}}(f;\mathbf{r};u)\mathtt{P}_\sigma(u)\,\mathrm{d}u \tag{17}$$

where $\mathbf{r}$ denotes the triplet (x, y, z).

Using Eq. (16), this mean is approximated by

$$\begin{aligned} m_{\hat{\mathbf{E}}}(f;\mathbf{r}) \simeq m_{\hat{\mathbf{E}}_n}(f;\mathbf{r}) &= \int_{\mathbb{R}} \hat{\mathbf{E}}_n(f;\mathbf{r};u)\mathtt{P}_\sigma(u)\,\mathrm{d}u \\ &= \sum_{i=0}^{n} \hat{\mathbf{E}}^i(f;\mathbf{r})I_i \end{aligned} \tag{18}$$

where

$$I_i = \int_0^{+\infty} \frac{\sqrt{u}\,e^{-\frac{1}{2}\sqrt{u/(b_f s^4)}}}{32(b_f s^4)^{\frac{3}{2}}} L_i(u)\,\mathrm{d}u \tag{19}$$

The above integral is evaluated using Gauss–Laguerre quadrature rule to obtain

$$I_i = \sum_{j=0}^{m} \psi_j L_i(\sigma_j) \tag{20}$$

with

$$\psi_j = \frac{1}{2}\frac{\Gamma(m+3)u_j}{m!(m+1)^2[\mathbf{L}_{m+1}^2(u_j)]^2}, \quad u_j = \frac{\sigma_j^{1/2}}{2s^2 b_f^{1/2}} \tag{21}$$

and where in practice $m = n$.

The points σ_j, $0 \leqslant j \leqslant n$, are the collocation points associated with the pdf of σ, Γ is the Gamma function and $\mathbf{L}_{m+1}$ is the $(m+1)$ order Laguerre polynomial.

Using the property (11) of Lagrange polynomials, we get $I_i = \psi_i$ and the n-approximation (18) of the mean takes the form

$$m_{\hat{\mathbf{E}}_n}(f;\mathbf{r}) = \sum_{i=0}^{n} \psi_i \hat{\mathbf{E}}^i(f;\mathbf{r}) \tag{22}$$

4.2.2. Approximation of the covariance matrix

By definition, the covariance matrix of the field $\hat{\mathbf{E}}$ is given by

$$C_{\hat{\mathbf{E}}}(f,\mathbf{r}) = \int_{\mathbb{R}} \hat{\mathbf{E}}(f;\mathbf{r};u)\hat{\mathbf{E}}^*(f;\mathbf{r};u)\mathtt{P}_\sigma(u)\,\mathrm{d}u - m_{\hat{\mathbf{E}}}(f;\mathbf{r})m^*_{\hat{\mathbf{E}}}(f;\mathbf{r}) \tag{23}$$

where $*$ is the symbol of the transpose conjugate.

Using (16) and (18) this matrix is approximated by

$$\begin{aligned} C_{\hat{\mathbf{E}}}(f,\mathbf{r}) \simeq C_{\hat{\mathbf{E}}_n}(f,\mathbf{r}) &= \int_{\mathbb{R}} \hat{\mathbf{E}}_n(f;\mathbf{r};u)\hat{\mathbf{E}}_n^*(f;\mathbf{r};u)\mathtt{P}_\sigma(u)\,\mathrm{d}u - m_{\hat{\mathbf{E}}_n}(f;\mathbf{r})m^*_{\hat{\mathbf{E}}_n}(f;\mathbf{r}) \\ &= \sum_{i=0}^{n}\sum_{j=0}^{n} \hat{\mathbf{E}}^i(f;\mathbf{r})\big(\hat{\mathbf{E}}^j(f;\mathbf{r})\big)^* I_{ij} - m_{\hat{\mathbf{E}}_n}(f;\mathbf{r})m^*_{\hat{\mathbf{E}}_n}(f;\mathbf{r}) \end{aligned} \tag{24}$$

where $m_{\hat{\mathbf{E}}_n}(f;\mathbf{r})$ is given by Eq. (18) and I_{ij} by

$$I_{ij} = \int_0^{+\infty} \frac{\sqrt{u}\, e^{-\frac{1}{2}\sqrt{u/b_f s^4}}}{32(b_f s^4)^{\frac{3}{2}}} L_i(u) L_j(u)\, \mathrm{d}u \tag{25}$$

Similarly, this integral can be evaluated using Gauss–Laguerre quadrature rule and we get

$$I_{ij} = \sum_{q=0}^{m} \psi_q \delta_{iq} \delta_{jq} \tag{26}$$

where ψ_q is given by Eq. (21). Taking $m = n$ and inserting Eq. (26) into Eq. (24) we finally obtain the following n-approximation of the covariance matrix:

$$C_{\hat{\mathbf{E}}_n}(f,\mathbf{r}) = \sum_{i=0}^{n} \psi_i \hat{\mathbf{E}}^i(f;\mathbf{r}) \big(\hat{\mathbf{E}}^i(f;\mathbf{r})\big)^* - m_{\hat{\mathbf{E}}_n}(f;\mathbf{r}) m^*_{\hat{\mathbf{E}}_n}(f;\mathbf{r}) \tag{27}$$

5. Application to LASMEA MSRC

5.1. Computation of the collocation points and convergence

The collocation points must be computed for every frequency because they depend on the scaling factor of the conductivity pdf which depends on the frequency (19). Fig. 3 shows the evolution of the conductivities as a function of the frequency for 4 points of collocation. For $n = 4$, the weights ψ_i (they are independent on the frequency) are given in Table 1.

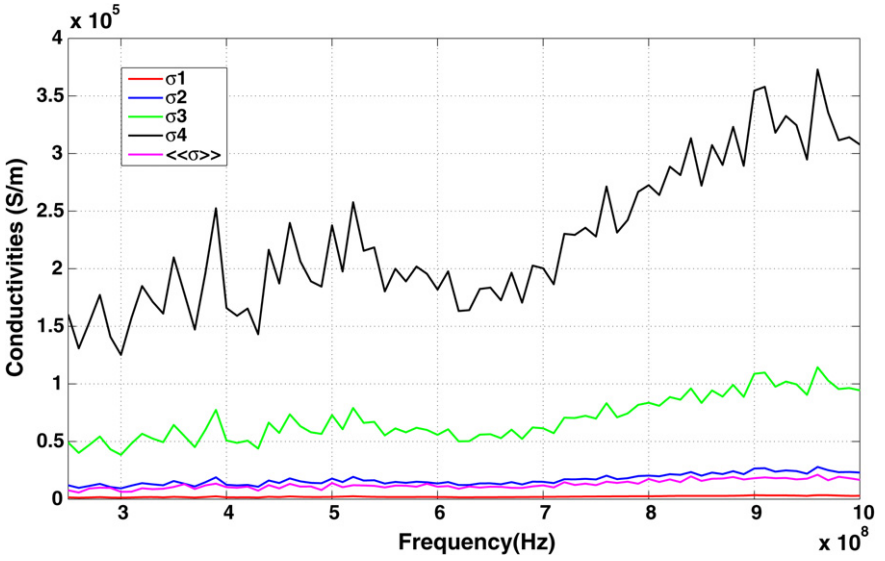

Fig. 3. Frequential evolution of conductivities for 4 collocation points and the corresponding weighted mean.

Table 1
Weights of the collocation points for $n = 4$.

Conductivity	Weights
σ_1	0.36
σ_2	0.53
σ_3	0.10
σ_4	2.18×10^3

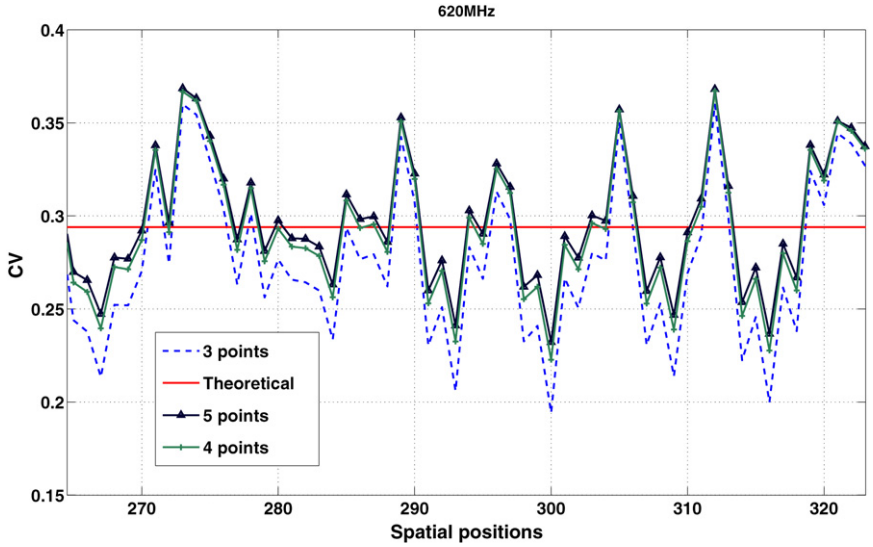

Fig. 4. Numerical coefficient of variation according to the number of collocation points used.

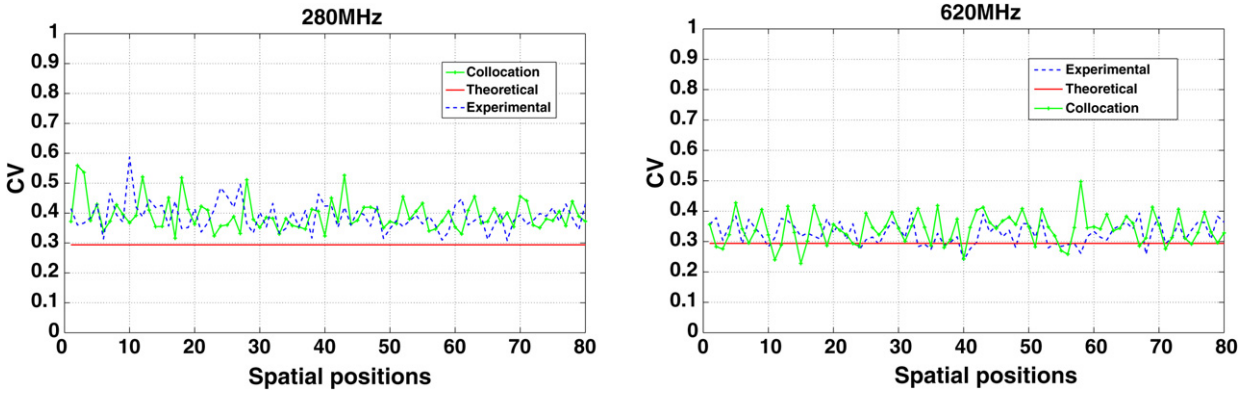

Fig. 5. Comparison between experimental and numerical CV of the modulus of the total electric field for 80 points into the working volume.

Note that only 4 points of collocation have been used for the computations, this being sufficient to get the convergence of results (see Fig. 4).

5.2. Simulation results

Fig. 5 shows that the CV of the modulus of $\hat{\mathbf{E}}$ is well approximated with only four deterministic computations. We can see that numerical results get closer to experimental results as the frequency increases, since Hill's hypothesis are better satisfied at high frequency. The CV may show fast variations since a small variation on the mean or the variance of the field can have a dramatic impact on that value. This explains the differences between experimental results and the results obtained by collocation. Moreover, the mean and the variance of the conductivity used to compute the collocation points have been obtained from experimental measures and by application of the ergodicity principle. This assumes that the parameters of the probability law are identical at any point of the working volume, which is not always true. However, the stochastic collocation gives better results than those obtained with 51 or 4080 values of the Monte Carlo simulation (see Fig. 2).

Finally, with the stochastic collocation method, we were able to compute the CV with only 4 simulations of the empty MSRC when standard techniques would have required 51 simulations of the MSRC with a stirrer.

Table 2
Comparison between experimental and numerical estimates of m_{cv} and σ_{cv}^2 for $f = 400$ MHz.

400 MHz	Experimental (80 points)	Collocation (80 points)
$\tilde{m}_{cv}$	0.3572	0.3185
I_β for $\beta = 90\%$	0.3510–0.3634	0.3124–0.3245
I_β for $\beta = 95\%$	0.3498–0.3646	0.3113–0.3257
I_β for $\beta = 99\%$	0.3475–0.3669	0.3090–0.3279
$\tilde{\sigma}_{cv}^2$	0.0336	0.0329
I_β for $\beta = 90\%$	0.02959–0.03843	0.02897–0.03763
I_β for $\beta = 95\%$	0.02892–0.0395	0.02832–0.03868
I_β for $\beta = 99\%$	0.02769–0.04175	0.02711–0.04088

5.3. Confidence interval of the CV of the electric field modulus

In order to quantify more precisely the differences between the two CVs (experimental and collocation) we use the confidence intervals of the mean and the variance for 80 points.

Let $0 \leqslant \beta \leqslant 1$ be a real number close to 1 and let $\tilde{a}$ be a point estimate of an unknown real parameter a. The confidence interval of a at the confidence level β is defined as the interval I_β of $\mathbb{R}$ such that the probability that I_β contains a is equal to β i.e. $P(I_\beta \ni a) = \beta$. This interval is of the form: $I_\beta = [\tilde{a} - \epsilon, \tilde{a} + \epsilon]$, where ϵ is a real number such that $P(|a - \tilde{a}| < \epsilon) = \beta$.

Here two parameters are considered: the mean m_{cv} and the variance σ_{cv}^2 of the coefficient of variation of the modulus of the total electric field. For n sufficiently large, the confidence intervals at the confidence level β of these parameters can be approximated by

- for m_{cv}

$$I_\beta \cong \left[\tilde{m}_{cv} - t_\beta \frac{\tilde{\sigma}_{cv}}{\sqrt{n}}, \tilde{m}_{cv} + t_\beta \frac{\tilde{\sigma}_{cv}}{\sqrt{n}}\right] \tag{28}$$

- for σ_{cv}^2

$$I_\beta \cong \left[\tilde{\sigma}_{cv}^2 - t_\beta \sqrt{\frac{2}{n-1}}\tilde{\sigma}_{cv}^2, \tilde{\sigma}_{cv}^2 + t_\beta \sqrt{\frac{2}{n-1}}\tilde{\sigma}_{cv}^2\right] \tag{29}$$

where $\tilde{m}_{cv}$ and $\tilde{\sigma}_{cv}^2$ are the values of m_{cv} and σ_{cv}^2 estimated from the n-sample of the CV and t_β is given by

$$t_\beta = \Phi^{-1}\left(\frac{1+\beta}{2}\right) \tag{30}$$

where Φ is the standard Gaussian distribution function defined by

$$\Phi(x) = \frac{1}{\sqrt{2\pi}} \int_{-\infty}^{x} \exp\left(\frac{-u^2}{2}\right) \mathrm{d}u, \quad x \in \mathbb{R} \tag{31}$$

These confidence intervals have been computed for the experimental and numerical (collocation) estimates of m_{cv} and σ_{cv}^2 and for two frequencies ($f = 400$ MHz, $f = 620$ MHz) and three values of β (0.90; 0.95; 0.99). The obtained results are shown in Tables 2 and 3. It can be seen that:

- for $f = 400$ MHz, the confidence intervals of the numerical and experimental estimates of m_{cv} do not overlap since the corresponding confidence intervals for σ_{cv}^2 overlap;
- for $f = 620$ MHz, these confidence intervals overlap in any case (i.e. for the three values of β) for m_{cv} and overlap only in the case $\beta = 0.99$ for σ_{cv}^2.

Table 3
Comparisons between experimental and numerical estimates of m_{cv} and σ^2_{cv} for $f = 620$ MHz.

620 MHz	Experimental (80 points)	Collocation (80 points)
$\tilde{m}_{cv}$	0.3271	0.3405
I_β for $\beta = 90\%$	0.3205–0.3339	0.3312–0.3498
I_β for $\beta = 95\%$	0.3192–0.33517	0.3294–0.35156
I_β for $\beta = 99\%$	0.3167–0.33767	0.32596–0.35504
$\tilde{\sigma}^2_{cv}$	0.0364	0.0505
I_β for $\beta = 90\%$	0.03205–0.04163	0.0445–0.058
I_β for $\beta = 95\%$	0.03133–0.04279	0.04346–0.05937
I_β for $\beta = 99\%$	0.03–0.04523	0.04161–0.0627

These results confirm the effectiveness of the collocation method especially for high frequencies. One can imagine using this approach for more complex MSRC simulations and in particular when an equipment under test is present in the working volume.

6. Conclusion

In this article, we have presented a new method for the estimation of statistical parameters of the electromagnetic field. We have proposed a probabilistic model of the MSRC based on an analogy between a rotating mode stirrer and the conductivity of the walls of the MSRC. The stochastic collocation method makes possible a simulation of the MSRC without stirrer and a direct introduction of losses in the resolution of Maxwell's equations using FDTD or other numerical methods. Results are obtained with a limited number of conductivity values and therefore a limited number of simulations of the empty cavity. Comparison with experimental measures shows that this method is valid in the optimal working range of the MSRC.

References

[1] M.L. Crawford, G.H. Koepke, Design, evaluation, and use of a reverberation chamber for performing electromagnetic susceptibility/vulnerability measurements, National Bureau of Standards, Technical Note 1092, Boulder, CO, 1986.
[2] J.F. Dawson, et al., Reverberation (mode-stirred) chambers for electromagnetic compatibility, EMC and Compliance 46 (2003) 30–38.
[3] C. Bruns, Three-dimensional simulation and experimental verification of a reverberation chamber, PhD Thesis, ETHZ Zurich, 2005.
[4] G. Orjubin, et al., On the FEM modal approach for a reverberation chamber analysis, IEEE Transactions on Electromagnetic Compatibility 49 (1) (2007) 76–85.
[5] B. Lizhou, Reverberation chamber modeling using FDTD, in: IEEE International Symposium on Electromagnetic Compatibility, Seattle, WA, USA, 1999, pp. 7–11.
[6] F. Moglie, Convergence of the reverberation chambers to the equilibrium analyzed with the finite-difference time-domain, IEEE Transactions on Electromagnetic Compatibility 46 (3) (2004) 469–476.
[7] P. Bonnet, et al., FDTD modelling of reverberation chamber, Electronics Letters 41 (20) (2005) 1101–1102.
[8] A. Coates, et al., Validation of a three-dimensional Transmission Line Matrix (TLM) model. Implementation of a mode-stirred reverberation chamber, IEEE Transactions on Electromagnetic Compatibility 49 (4) (2007) 734–744.
[9] D.A. Hill, A reflection coefficient derivation for the Q of a reverberation chamber, IEEE Transactions on Electromagnetic Compatibility 38 (4) (1996) 591–592.
[10] F. Diouf, Application de méthodes probabilistes à l'analyse des couplages en compatibilité électromagnétique et contribution à la sûreté de fonctionnement de systèmes électroniques, PhD Thesis, Université Clermont II, 2008.
[11] J.H. Beggs, et al., Finite-difference time-domain implementation of surface impedance boundary conditions, IEEE Transactions on Antennas and Propagation 40 (1) (1992) 49–56.
[12] C. Chauvière, J.S. Hesthaven, L. Wilcox, Efficient Computation of RCS from Scatterers of Uncertain Shapes, IEEE Transactions on Antennas and Propagation 55 (5) (2007) 1437–1448.